

# Self-organisation through layering of $\beta$ -plane like turbulence in plasmas and geophysical fluids

P. L. Guillon<sup>1,2</sup>, G. Dif-Pradalier<sup>3</sup>, Y. Sarazin<sup>3</sup>, D. W. Hughes<sup>4</sup>, Ö. D. Gürçan<sup>1</sup>

<sup>1</sup>*Laboratoire de Physique des Plasmas, CNRS, Ecole Polytechnique, Sorbonne Université, Université Paris-Saclay, Observatoire de Paris, F-91120 Palaiseau, France*

<sup>2</sup>*ENPC, Institut Polytechnique de Paris, 77455 Champs-sur-Marne, Marne-la-Vallée cedex 2, France*

<sup>3</sup>*CEA, IRFM, F-13108 Saint-Paul-lez-Durance, France and*

<sup>4</sup>*School of Mathematics, University of Leeds, Leeds LS2 9JT, UK*

Staircase formation and layering is studied in simplified, potential vorticity conserving models of plasmas and geophysical fluids, by investigating turbulent self-organisation and nonlinear saturation with different mechanisms of free energy production — forcing or linear instability — and with standard or modified zonal flow responses. To this end, staircase formation in both the standard and modified Charney-Hasegawa-Mima equations with stochastic forcing, along with two different simple instability driven models — one from a plasma and from a geophysical context — are studied and compared. In these studies, it is observed that  $\beta$ -plane turbulence that does not distinguish between zonal and non-zonal perturbations (i.e., standard zonal response) gradually forms large-scale, elliptic zonal structures that merge progressively, regardless of whether it is driven by forcing (though it should be slow enough to allow wave couplings) or by the baroclinic instability, using for example a two-layer model. Conversely, the plasma system, with its modified zonal response, can rapidly form straight, stationary jets of well-defined size, again regardless of the way it is driven: by stochastic forcing or by the dissipative drift instability. Furthermore, the instability-driven plasma system exhibits a phase transition between a zonal flow dominated state and an eddy dominated state. In both states, saturation is possible without large-scale friction.

## I. INTRODUCTION

The similarities between basic descriptions of turbulence in geophysical fluids and tokamak plasmas have been known for a while [1]. They are both quasi-two-dimensional systems, which become so by the effects of gravity and strong planetary rotation in one case, and the confining background magnetic field in the other. Two key elements of this similarity are the fact that the Coriolis force and the Lorentz force have the same structures, i.e., they are the cross product of a velocity and a frequency (Earth's rotation or cyclotron pulsation in the electrostatic limit) along a normal direction defined by hydrostatic balance or MHD equilibrium. Both systems are in static equilibrium, on top of which fluctuations may appear. They also exhibit significant large-scale inhomogeneities, thereby resulting in very anisotropic turbulence, characterised by wave-like dynamics, whose nonlinear modulations then favour the formation of zonal flows (ZFs) [2, 3] and layering of the initial inhomogeneities [4, 5].

Even though the physical details of the two problems are vastly different, with some of these differences being of great importance for the goals of those subsequent disciplines, in their simplest form, the turbulence in both systems can be described using a common framework, represented by the so-called Charney-Hasegawa-Mima (CHM) equations [6, 7]. In this framework, one can define a conserved quantity, known as the potential vorticity (PV), whose gradients are responsible for the corresponding waves — Rossby waves for geophysical fluids and drift waves for plasmas — and whose non-linear evolution gives rise to  $\beta$ -plane turbulence [8].

In this simple form, the PV can be 'inverted' [9, 10], or written as a function of the velocity field, which can in turn be written in terms of the stream function (or the electrostatic potential for the plasma case, which has the same role apart from its units), thus closing the loop. However, the simplest  $\beta$ -plane models do not generate turbulence spontaneously and have to be driven by external forcing. This is usually justified in the geophysical fluid dynamics (GFD) context by arguing that perturbations due to different physical mechanism, such as the baroclinic instability, inject energy at small scales, which then piles up towards larger scales for which the  $\beta$ -plane approximation is relevant. Unfortunately in the plasma case, there does not seem to be such scale separation between where, for example, a drift instability would inject its energy, and the scales at which the drift wave turbulence would appear, except in rather unlikely scenarios, such as the energy from an electron instability (e.g., the electron temperature gradient driven mode [11]) somehow cascading towards large scales to generate drift wave turbulence. Note that for the geophysical problem, the characteristic length scale of the perturbations tends to be smaller than the characteristic scale of the underlying dynamics — the Rossby deformation radius — whereas for the plasma problem, it tends to be larger than the corresponding scale — the Larmor radius. In table I, we give a summary of the analogy between the geophysical and plasma problems. The coordinate system of both problems is illustrated in figure 1. In particular, note that the  $x$  and  $y$  directions are somewhat interchanged in the two problems,  $x$  ( $y$ ) being the periodic direction in the geophysical (plasma) context. Also, as discussed later, instabilities arise due to gradients in the  $y$  ( $x$ ) direction in the

| Physical context           | Geophysical problem  | Plasma problem                                       |
|----------------------------|--|--|
| Driving force/vector field | Coriolis/ $\Omega_p$   | Lorentz/ $\mathbf{B}$                                |
| PV gradient direction      | $y$ (north-south)  | $x$ (radial)   |
| Zonal direction            | $x$ (east-west)  | $y$ (poloidal)                                       |
| PV gradient                | Planetary vorticity $\beta = df/dy$                                | Plasma density $\kappa = -dn/dx$                     |
| Characteristic length      | Rossby deformation radius<br>$R = \sqrt{gh}/f_0$                   | Ion sound Larmor radius<br>$\rho_s = c_s/\Omega_i$   |
| Small parameter            | Rossby number $U/(Lf_0)$   | $\rho_s/L_n$   |
| Advective velocity         | geostrophic (3)  | $\mathbf{E} \times \mathbf{B}$ (10)                  |
| $\beta$ -plane model       | Charney-Hasegawa-Mima  | Generalised Hasegawa-Mima                            |
| Corresponding PV           | $q = \nabla^2\psi - \psi + \beta y$                                | $q = \tilde{\Phi} - \nabla^2\Phi - \kappa x$         |
| Characteristic freq.       | Rossby waves freq.<br>$\omega_k = \beta k_x/(1+k^2)$               | Drift waves freq.<br>$\omega_k = \kappa k_y/(1+k^2)$ |
| Minimal unstable model     | Two-layer quasi-geostrophic  | Hasegawa-Wakatani                                    |
| Instability source         | Velocity shear<br>between the two layers                           | Non-adiabatic electron<br>response due to collisions |
| Perturbed PV               | $q'_{1,2} = \nabla^2 q_{1,2} \pm F_{1,2}(\psi_{2,1} - \psi_{1,2})$ | $q' = n - \nabla^2\Phi$                              |

Table I. Summary of the analogy between the geophysical and plasma problems.

GFD (plasma) context.

In this study, we focus mainly on the observation of fundamental differences in layering between  $\beta$ -plane like systems that are driven by instability or by external forcing. In particular, the instability-driven system is able to self-regulate, not only the turbulence, but also the energy injection, essentially by the influence of ZFs on the linear instability that drives the turbulence. External forcing (either local in configuration space or local in scale, in Fourier space), by contrast, keeps injecting energy even in a saturated state, and forces the system to somehow find a way to dissipate the energy/enstrophy that is being pumped continuously into the system.

For the forced  $\beta$ -plane case, we consider two different kinds of zonal flow evolution. In the standard CHM system, the conserved dimensionless PV is defined as  $q = \psi - \zeta + \beta y$ , in terms of the stream function  $\psi$  and the vorticity  $\zeta \equiv \nabla^2\psi$ , which means that the large-scale zonal PV is proportional to the zonally averaged stream function (i.e.,  $\langle q \rangle_x \approx \langle \psi \rangle_x + \beta y$  as  $\partial_x \rightarrow 0$ ). On the contrary, in the generalised Hasegawa-Mima (GHM) system [12] relevant for fusion plasmas, the PV is defined as  $q = \tilde{\Phi} - \nabla^2\Phi - \kappa x$ , with  $\Phi$  being the non-dimensional electrostatic potential (which plays the role of the stream function) and where  $\kappa$  is the equivalent of  $\beta$  but with the zonal direction being  $y$  instead of  $x$ . In the plasma case, only the non-zonal part of the stream function,  $\tilde{\Phi} \equiv \Phi - \langle \Phi \rangle_y$ , plays a role in the PV. As a consequence, the large-scale zonal PV for the GHM is vorticity, instead of the stream function (i.e.,  $\langle q \rangle_y \approx -\partial_x^2 \langle \Phi \rangle_y - \kappa x$  as  $\partial_x \rightarrow 0$ ). This slightly different form of the zonal PV is actually a consequence of the zonal flow response. In the plasma problem, when drift wave perturbations have a finite parallel gradient along the guiding magnetic field, the electrons move rapidly in the parallel direction, causing the difference between density and electrostatic potential to decay. This is called the electron response. However ZFs, in the plasma problem, vary only in the radial ( $x$ ) direction. This means that, as they have no parallel perturbations, they are unaffected by the electron response, and hence zonal density and zonal electrostatic potential remain independent of one another. This

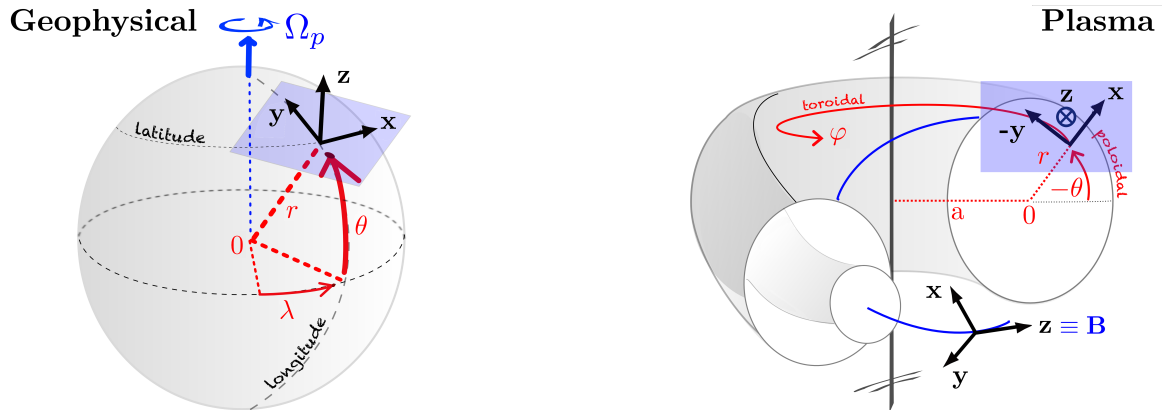


Figure 1. Summary of the various geometries and conventions used in the geophysical and plasma problems.

| Model                                  | $\beta$ -plane/CHM       | GHM                          | Two-layer QG               | HW                           |
|--|--------------------------|------------------------------|----------------------------|------------------------------|
| Forcing                                | Small scale stochastic   |                              | Linear instability         |                              |
| Equation(s)                            | (7)                      | (14)                         | (24) & (25)                | (18) & (19)                  |
| Zonal response                         | Standard                 | Modified                     | Standard                   | Modified                     |
| Layering                               | Elliptic jets<br>merging | Straight jets<br>finite size | Elliptic jets<br>modulated | Straight jets<br>finite size |
| Zonal to total<br>kinetic energy ratio | $36.4 \pm 1.0\%$         | $97.3 \pm 0.3\%$             | $24.3 \pm 0.9\%$           | $91.5 \pm 0.3\%$             |

Table II. The different models examined in the article, their corresponding forcing, zonal response and observed layering, with the fraction of zonal to total kinetic energy averaged over the last quarter of each simulation.

is called the *modified* ZF response, and it causes large-scale zonal modes to have minimum inertia. As will be shown, the difference in zonal response has drastic consequences on turbulence self-organisation properties.

We then consider two examples of instability-driven  $\beta$ -plane turbulence models: the Hasegawa-Wakatani model [13], which is considered as a minimal model of plasma turbulence and ZFs, with drift waves driven by a dissipative drift instability, and the two-layer quasi-geostrophic (QG) model [14, 15], which is a minimal representation of the baroclinic instability. The former, arising from a plasma problem, has the modified zonal response, while the latter being a GFD model, incorporates a standard zonal response (i.e., ZFs are not treated differently from the other modes). The mechanisms of instability are also very different, since it is the non-adiabatic electron response in the parallel direction that activates the dissipative drift instability, whereas the particular form of the two-layer model that we consider relies on a vertically sheared background zonal (east-west) flow that is modelled as a discontinuity between the two layers.

Nevertheless, in both models, even though the turbulence may be described using only two dimensions, the instabilities require three-dimensional effects. For tokamak plasmas [16], which are more or less periodic in the third dimension, these can be introduced by considering a finite wave-number, and a finite electron mobility in this direction, resulting in the minimal Hasegawa-Wakatani model. In contrast, in the GFD case [17], the minimal three dimensionality necessary to describe the baroclinic instability in planetary atmospheres is introduced by the two-layer QG model, in which the vertically stacked layers have differing background zonal velocities as well as densities, resulting in an inverted PV profile. This underlines once again how the two systems are very different in details related to geometry, forcing and boundary conditions, while being very similar in terms of the underlying nonlinear structure of the equations.

The different models examined in the article, their corresponding forcing, zonal response and observed layering are given in table II. As a short summary of our results, we find that for forced  $\beta$ -plane turbulence driven at small-scales by stochastic forcing and with *standard* zonal response (i.e., CHM driven at small scales), the forcing amplitude and time scale (i.e., the time step of the random forcing) require tuning to achieve layering. If the system is forced weakly and sufficiently slowly, the ZFs form in stages, as suggested by the wave turbulence picture [18–20]. We note, however, that if the forcing is too rapid or too strong, 2D Navier-Stokes like behaviour is instead observed. On the contrary, for the GHM system, where the zonal response is *modified*, we observe the rapid formation of straight stationary ZFs, whose size is well defined and does not seem to change in time, over the time scales of the simulations. The contrast between the standard zonal response, which generates layering with low non-zonal modes coming along with purely zonal modes, and the modified response, which results in a purely zonal pattern, is illustrated in table II by the fraction of zonal to total kinetic energy, which accounts only for purely zonal modes.

In the two-layer model, which has the standard response, the saturated state is again dominated by strong elliptic ZFs that are modulated and seem to play the role of wave-guides for the remaining Rossby waves [21]. By contrast, in the Hasegawa-Wakatani system, two major regimes can be reached: either a ZF-dominated regime or a 2D turbulence regime without flows, depending on the ratio of two linear parameters, the adiabatic coupling  $C$  and the mean density (i.e., PV) gradient  $\kappa$ . For  $C/\kappa > 0.1$ , one finds a state that is dominated by ZFs at large scales, and displays characteristic features of a two-dimensional forward enstrophy cascade at small scales. Since we choose not to introduce zonal flow damping unless necessary, the saturated state has zero net Reynolds power — i.e., the energy transfer associated with the Reynolds stress. Thus, once established, the flows turn off the energy drive, and the system ends up in a fixed-point-like stationary state, with straight jets having a well-defined spatial scale. The Hasegawa-Wakatani system is also well known to exhibit an abrupt transition, with a hysteresis loop, from a zonally dominated state to a state of two-dimensional turbulence as its linear control parameter  $C/\kappa$  is varied [22–24]. Note, however, that extending this observation to gyrokinetic systems where turbulence is driven by the ion temperature gradient instability or trapped electron modes remains unclear [25].

The rest of the paper is organised as follows. In §II we introduce the different models based on PV conservation, and their corresponding minimal models with instability, which drive turbulence and then layering. In §III we

examine the layering process in  $\beta$ -plane turbulence (*via* CHM, two-layer QG and GHM models), which can be forced either randomly at small scales, or coherently at large scale *via* a linear instability mechanism. In §IV we detail the instability-driven plasma case, discussing the formation of ZFs in the HW system, which have a finite size without large-scale friction and which turn off the linear drive.

## II. MODELS FOR GEOPHYSICAL AND PLASMA TURBULENCE

In this section, we define the four different models based on  $\beta$ -plane turbulence that exhibit layering at the most simple level. First, in §III A, we start from PV conservation to derive the standard Charney-Hasegawa-Mima (CHM) model, and its equivalent in the plasma context, which has the modified zonal response — the Generalised Hasegawa-Mima (GHM) system. Both of these models have to be forced at small scales in order to generate 2D turbulence that then develops layering. We then go on to discuss how the responses can affect the layering.

Then, in §III B, we consider the minimal models in the  $\beta$ -plane framework where the energy is injected self-consistently through a linear instability: the Hasegawa-Wakatani model in the plasma context (which has the modified zonal response), and the two-layer quasi-geostrophic (QG) model in the GFD case (which has the standard zonal response).

### A. PV conservation and $\beta$ -plane turbulence

#### 1. Geophysical problem

For a fluid in large scale equilibrium around a planet, such as the atmosphere or ocean, gravity  $g\hat{z}$  is balanced by the vertical pressure gradient  $\partial_z P$ , in what is known as hydrostatic balance. This naturally links the fluid pressure variations to variations in height through a barometric relation such as  $\Delta P = -\rho g \Delta h$ . The basic equation for a rotating fluid in such a vertical hydrostatic balance is the Navier-Stokes equation, written in a rotating frame:

$$(\partial_t + \mathbf{u} \cdot \nabla) \mathbf{u} + 2\boldsymbol{\Omega}_p \times \mathbf{u} = -\frac{\nabla P}{\rho} - g\hat{z} + \nu \nabla^2 \mathbf{u}, \quad (1)$$

where the last term on the left hand side represents the Coriolis force due to planetary rotation  $\boldsymbol{\Omega}_p$ . While the hydrostatic balance defines a direction  $\hat{\mathbf{n}}$  normal to the atmosphere, which can be used to naturally decompose the motion of the fluid into parallel and perpendicular directions, the background rotation  $\boldsymbol{\Omega}_p$  defines a second axis. Considering the projection of the planetary vorticity implied by the rotation of the planet onto the direction normal to the atmosphere, one defines

$$f \equiv 2\boldsymbol{\Omega}_p \cdot \hat{\mathbf{n}} = 2\Omega_p \sin \theta, \quad (2)$$

where  $\theta$  is the latitude. The  $\beta$ -plane can then be defined as a tangential plane at a (central) latitude  $\theta$ , with the local coordinates  $x$  and  $y$  corresponding to zonal (east) and meridional (north) directions (see figure 1 for an illustration).

For strong rotation (characterised by small Rossby number  $Ro$ , where  $Ro$  is the ratio of inertial to Coriolis forces), the principal (geostrophic) balance is between the Coriolis force and the horizontal pressure gradient; this represents a balance between fluctuating fields, in contrast to the hydrostatic balance between equilibrium quantities. Geostrophic balance, together with the barometric relation between pressure and height, can be used to write [26]

$$\mathbf{u}_\perp = \frac{\hat{\mathbf{n}} \times \nabla P}{f\rho} = \frac{g}{f} \hat{\mathbf{n}} \times \nabla h, \quad (3)$$

thus implying that the height  $h$  plays the role of the stream function  $\psi$  (i.e., as in  $\mathbf{u} = \hat{\mathbf{n}} \times \nabla \psi$ ). Note that this relation can formally be obtained as the leading order term in a small Rossby number expansion of the Navier-Stokes equation.

The key aspect of the  $\beta$ -plane model is the assumption that Eqn. (2) can be expanded in a Taylor series about the central latitude  $\theta$ , as  $f = f_0 + \beta y$ , with  $\beta = df/dy|_\theta$ . On defining the relative vorticity in the normal direction as  $\zeta = \hat{\mathbf{n}} \cdot (\nabla \times \mathbf{u})$ , and using the continuity equation for the layer thickness, one can show that

$$\frac{d}{dt} \left( \frac{\zeta + f}{h} \right) = 0. \quad (4)$$

Eq. (4) represents the conservation of PV,  $q = (\zeta + f)/h$ , implying that the total vorticity (fluid + planetary) and the height of the fluid increase or decrease together.

On writing  $h = h_0 + h_1$ , together with  $f = f_0 + \beta y$ , with  $h_1/h_0$  and  $\beta y/f_0$  coming into play at the same order in the small Rossby number expansion (e.g., see [26]), the PV takes the form

$$q = \frac{\zeta + f_0 + \beta y}{h_0 + h_1} \approx \frac{\zeta + f_0 + \beta y - f_0 h_1/h_0}{h_0}. \quad (5)$$

Using (3) with this expansion to define  $\psi \equiv (g/f_0) h_1$ , and removing the constant  $f_0/h_0$ , yields

$$q \approx h_0^{-1} (\nabla^2 \psi + \beta y - R^{-2} \psi), \quad (6)$$

with  $R \equiv \sqrt{g\bar{h}}/f_0$ , the Rossby deformation radius, defining a characteristic length scale and  $f_0^{-1}$  a characteristic time scale. On defining  $x/R \rightarrow x$ ,  $f_0 t \rightarrow t$ ,  $\psi R^2/f_0 \rightarrow \psi$ , and  $R\beta/f_0 \rightarrow \beta$  as dimensionless variables, and rescaling the PV by  $h_0$ , the non-dimensional form of the Charney-Hasegawa-Mima (CHM) equation can be written as

$$\frac{dq}{dt} = \partial_t (\psi - \nabla^2 \psi) - \beta \partial_x \psi = (\hat{\mathbf{n}} \times \nabla \psi) \cdot \nabla (\nabla^2 \psi), \quad (7)$$

where  $q = \nabla^2 \psi - \psi + \beta y$  is the potential vorticity. By adding forcing and dissipation, we obtain the forced  $\beta$ -plane model,

$$(\partial_t + (\hat{\mathbf{n}} \times \nabla \psi) \cdot \nabla) q = \mathbf{f}_q + \nu \nabla^2 q, \quad (8)$$

where  $\mathbf{f}_q$  is the forcing and  $\nu \nabla^2 q$  is the dissipation. It is also common to explore the large  $R$  limit by replacing the fluctuating part of  $q$  by  $\zeta$ .

## 2. Plasma problem

In contrast to hydrostatic balance in the geophysical problem, the large-scale balance in the plasma problem is represented by the MHD equilibrium between the Lorentz ( $\mathbf{J} \times \mathbf{B}$ ) force, due to equilibrium magnetic fields and currents, and the background pressure gradient. This equilibrium imposes a direction  $\hat{\mathbf{b}}$  in the direction of the equilibrium magnetic field, which can be used to separate the motion parallel and perpendicular to the magnetic field. In the plasma framework, the local coordinate  $x$  corresponds to the radial (from tokamak core to the edge) and  $y$  to the poloidal, or bi-normal direction (i.e.,  $\hat{\mathbf{y}} = \hat{\mathbf{b}} \times \hat{\mathbf{x}}$  is roughly poloidal). The toroidal direction, parallel to the magnetic field, is denoted by  $z$  (see figure 1 for an illustration). Contrary to the GFD case, the PV gradient here is along  $x$  and zonal flows are uniform along the  $y$  direction.

Considering ions as a fluid, the ion equation of motion takes the form

$$(\partial_t + \mathbf{u}_i \cdot \nabla) \mathbf{u}_i = -\frac{\nabla P}{m_i n_i} + \frac{e}{m_i} (\mathbf{E} + \mathbf{u}_i \times \mathbf{B}), \quad (9)$$

where the ion velocity  $\mathbf{u}_i$  is a sum of drift velocities. The MHD stationary equilibrium follows by considering ions and electrons together as a single fluid in static equilibrium. Using a formal drift expansion in a strong magnetic field (i.e., with the ratio of the inverse characteristic time scale to the cyclotron frequency being the small parameter), the leading order term is the  $\mathbf{E} \times \mathbf{B}$  drift velocity, which can be written as

$$\mathbf{u}_E = \frac{\hat{\mathbf{b}} \times \nabla \Phi}{B} = \hat{\mathbf{b}} \times \nabla \left( \frac{e\Phi}{T} \right) \rho_s c_s, \quad (10)$$

where the sound speed  $c_s = \sqrt{T_e/m_i}$ , the sound Larmor radius  $\rho_s = c_s/\Omega_i$  and  $\Omega_i = eB/m_i$  the ion cyclotron frequency. The last two quantities define respectively the spatial and temporal scales of the problem. The plasma, considered as a fluid, moves with the  $\mathbf{E} \times \mathbf{B}$  velocity, since both ions and electrons move together at that speed in the same direction. Comparing (10) with (3), we see that the geostrophic balance and the  $\mathbf{E} \times \mathbf{B}$  drift velocity  $\mathbf{u}_E$  have the same structure. The stream function role in the plasma problem is now played by the electrostatic potential  $\Phi$ .

To derive the  $\beta$ -plane equivalent in the plasma context, one usually starts by considering the equation of continuity (see, e.g., [1, 7] for a complete derivation),

$$(\partial_t + \mathbf{u}_E \cdot \nabla) n = \frac{1}{e} \nabla_{\parallel} J_{\parallel}, \quad (11)$$

where the plasma density is  $n = n_e = n_i$  due to quasi neutrality, and  $\nabla_{\parallel} J_{\parallel} = \nabla_{\parallel} (enu_{\parallel,e})$  corresponds to the electron current in the direction parallel to  $\mathbf{B}$ . Here we assume a uniform and constant magnetic field  $\mathbf{B}$ , and constant electron temperature  $T_e$ , so that the divergence of the particle flux reduces to  $\mathbf{u}_E \cdot \nabla n$ . Then, charge conservation, together with the assumption of cold ions (i.e.,  $T_i = 0$ ), and keeping the first term in the small parameter  $\rho_s/L_n$  expansion, where  $L_n$  is the characteristic length of the density gradient, leads to the vorticity equation,

$$-n\rho_s^2 (\partial_t + \mathbf{u}_E \cdot \nabla) \nabla^2 \left( \frac{e\Phi}{T_e} \right) = \frac{1}{e} \nabla_{\parallel} J_{\parallel}, \quad (12)$$

where the left hand side accounts for the divergence of the so-called ion polarisation current.

To further simplify the system, one uses the parallel component of Ohm's law without collisions, which gives  $\nabla_{\parallel} P = en\nabla_{\parallel} \Phi$ , thus relating parallel variations of pressure  $P$  and electrostatic potential  $\Phi$ . In combination with the ideal gas equation of state  $P = nT$ , with  $T$  understood as thermal energy, we obtain the so-called *adiabatic* electron response:

$$\frac{\tilde{n}}{n_0} \approx \frac{e\tilde{\Phi}}{T}. \quad (13)$$

In the plasma problem, the break down of the adiabatic electron response gives rise to various drift instabilities. Even though there exists a variety of different mechanisms leading to the break down of adiabaticity, resulting in different kinds of drift instabilities, here, in § III B, we consider only the effect of collisions in the parallel direction, as a minimal example of the dissipative drift instability. But first, we assume that the adiabatic electron response (13) holds, so that we obtain the equivalent of the  $\beta$ -plane model in the plasma problem.

The fact that the adiabatic electron response (13) applies only for non-zonal fields, i.e.,  $\tilde{\Phi} = \Phi - \langle \Phi \rangle_y$  and  $\tilde{n} = n - \langle n \rangle_y$ , underlines a non-trivial feature of the plasma geometry. In the plasma problem, ZFs are constant on magnetic flux surfaces (i.e., along  $y$  and in the  $\hat{\mathbf{b}}$  direction), and they vary only in the radial (i.e.,  $x$  in the plasma convention) direction. Hence, while the non-zonal modes, which are denoted by  $\tilde{\Phi}$  above, vary in all three directions and their variation in the parallel direction is governed by the adiabatic electron response, zonal perturbations are unaffected by this response. In a sense, electrons cannot respond to (zonal) perturbations that they do not see (their small gyro-radius does not allow them to feel radial-only perturbations). As such, zonal electrostatic potential and zonal density behave independently of each other. This is the physical basis of the *modified* zonal flow response for the plasma problem; as a consequence, the PV definition is slightly modified, as shown below.

To derive the  $\beta$ -plane plasma model, we take the zonal density  $\bar{n} \equiv \langle n \rangle_y = 0$ . We can thus expand  $n = n_0(-x/L_n + \tilde{n})$ , taking a mean profile linearly decreasing as a function of radius, while  $\Phi = \bar{\Phi} + \tilde{\Phi}$ , where  $\bar{\Phi} \equiv \langle \Phi \rangle_y$  is the zonal electrostatic potential. Using the adiabatic electron response, and combining Eqns (11) and (12), we obtain the so-called generalised-Hasegawa-Mima equation [12, 27], which can be written in non-dimensional variables  $e\Phi/T \rightarrow \Phi$ ,  $x/\rho_s \rightarrow x$ ,  $y/\rho_s \rightarrow y$  and  $\Omega_i t \rightarrow t$  as

$$\frac{dq}{dt} = \left( \partial_t + \hat{\mathbf{b}} \times \nabla \Phi \cdot \nabla \right) \left( \tilde{\Phi} - \nabla^2 \Phi \right) + \kappa \partial_y \Phi = 0, \quad (14)$$

where  $\kappa \equiv -\rho_s \frac{1}{n_0} \frac{dn_0}{dx} = \rho_s/L_n$  is the mean density gradient. In this case, the conserved PV has the form  $q = \tilde{\Phi} - \nabla^2 \Phi - \kappa x$ , with the common sign convention in the plasma community. Note that here,  $\rho_s$  is usually a small parameter and therefore the vorticity term is a small correction to the density term at large scales.

### 3. Standard and modified zonal flow responses

Considering their 3D structure, in the GFD problem, zonal perturbations are invariant in the  $x$  (i.e., east-west) direction, so they vary only in the  $y$  (i.e., north-south) direction, but there is nothing special about their variation in the direction normal to the atmosphere; they vary together with the other modes through the relation to fluid height. Hence, the zonal PV is  $\langle q \rangle_x = \nabla^2 \psi - \psi + \beta y$ , and, consequently, the time evolution of the zonal component of the stream function  $\bar{\psi}$  in Fourier space can be written from Eqn. (7) as

$$\partial_t \bar{\psi}_k = \frac{\mathcal{F}_k[\langle \hat{\mathbf{n}} \times \nabla \psi \cdot \nabla \nabla^2 \psi \rangle_x]}{1 + k^2}, \quad (15)$$

where  $\bar{\psi}_k$  is the Fourier component of  $\bar{\psi}$  with zonal wave vector  $\mathbf{k} = (0, k_y)$ , and  $\mathcal{F}_k$  is the Fourier transform operator to the  $k$  mode. This corresponds to the *standard* zonal response.

On the contrary, in the plasma problem, as previously discussed, the zonal PV is modified owing to the adiabatic electron response (13) applying only to non-zonal perturbations, and becomes  $\langle q \rangle_y = -\nabla^2 \bar{\Phi} - \kappa x$ . As such, using (14), the time evolution of the zonal Fourier component  $\bar{\Phi}_k$  of the electrostatic potential (where now  $\mathbf{k} = (k_x, 0)$  in the plasma problem coordinates) is described by

$$\partial_t \bar{\Phi}_k = -\frac{\mathcal{F}_k[\langle \hat{\mathbf{b}} \times \nabla \Phi \cdot \nabla \nabla^2 \Phi \rangle_y]}{k^2}, \quad (16)$$

which constitutes the *modified* zonal response. The main difference with the GFD case (15) is that for large-scale ZFs, i.e.,  $k \rightarrow 0$ , the right hand side of (16) grows as  $1/k^2$ , whereas it remains bounded for the standard zonal response (i.e.,  $1/(1+k^2) \rightarrow 1$ ). Therefore, it is said that ZFs have more *inertia* in standard  $\beta$ -plane turbulence, as opposed to the plasma case with the modified response, where they are much more easily excited, especially at large scales, which can explain why the flows are straighter and more easily formed.

## B. Minimal models with instability-driven turbulence

Both CHM and GHM models allow for the propagation of waves, respectively Rossby and drift waves, which are linearly stable. Therefore, to generate turbulence and consequently layering, one has to force the systems — e.g., stochastically at small scales.

Another mechanism for energy injection, which is physically more relevant, especially for the plasma case, is a linear instability. In the following, we consider the minimal model based on  $\beta$ -plane turbulence featuring a linear instability: the Hasegawa-Wakatani system for the plasma problem, which has the modified zonal response, and the two-layer quasi geostrophic model for the geophysical case, which has the standard zonal response.

### 1. Plasma case: the Hasegawa-Wakatani model

As we mentioned in the previous section, breaking of the adiabatic electron response in the parallel direction (13) promotes drift-wave instabilities; one of the simplest ways this can happen is through finite electron mobility — or non-zero resistivity  $\eta$ . In this case, Ohm's law in the parallel direction yields a parallel current

$$J_{\parallel} = \frac{T}{e\eta} \nabla_{\parallel} \left( \frac{e}{T} \tilde{\Phi} - \frac{\tilde{n}}{n_0} \right), \quad (17)$$

which we can insert into the right hand sides of Eqns (11) and (12).

We can then write the density equation in dimensionless variables as before, now using  $n_0(-\kappa x + \bar{n}(x, t) + \tilde{n}(x, y, t))$  as total density:

$$\left( \partial_t + \hat{\mathbf{b}} \times \nabla \Phi \cdot \nabla \right) n + \kappa \partial_y \tilde{\Phi} = C \left( \tilde{\Phi} - \tilde{n} \right), \quad (18)$$

where we have assumed a single dominant  $k_{\parallel}$  (e.g.,  $\tilde{\Phi}(x, y, z) \propto \tilde{\Phi}(x, y) \cos k_{\parallel} z$ ) in order to define  $C \equiv v_{te}^2 k_{\parallel}^2 / (\nu_c \Omega_i)$  as a model parameter, where  $\nu_c$  is the collision frequency (which sets the resistivity  $\eta = m_e \nu_c / e^2 n_0$ ) and  $v_{te}$  is the electron thermal velocity. Similarly, the non-dimensionalised vorticity equation becomes

$$\left( \partial_t + \hat{\mathbf{b}} \times \nabla \Phi \cdot \nabla \right) \zeta = C \left( \tilde{\Phi} - \tilde{n} \right), \quad (19)$$

where  $\zeta = \nabla^2 \Phi$  is the vorticity. Equations (18) and (19) together constitute the inviscid version of the Hasegawa-Wakatani system. Subtracting Eqn. (19) from (18) yields the equation of PV conservation,

$$\frac{dq}{dt} = \left( \partial_t + \hat{\mathbf{b}} \times \nabla \Phi \cdot \nabla \right) q' + \kappa \partial_y \Phi = 0, \quad (20)$$

where  $q = q' - \kappa x$  with  $q' = n - \zeta$  the perturbed PV. In this case, the modified zonal response manifests through the coupling term  $C(\tilde{\Phi} - \tilde{n})$ , where  $C$  is known as the *adiabaticity* parameter. Considering the linearised time evolution of  $(\tilde{n} - \tilde{\Phi})$  in Fourier space, we obtain

$$\partial_t \left( \tilde{n}_k - \tilde{\Phi}_k \right) + i\kappa k_y \tilde{\Phi}_k = -C \left( 1 + \frac{1}{k^2} \right) \left( \tilde{n}_k - \tilde{\Phi}_k \right), \quad (21)$$

where  $k$  is a non-zonal wave-number (i.e., with  $k_y \neq 0$ ), which means that the electron adiabatic response (13) is recovered at a rate  $C(1 + 1/k^2)$  for non-zonal perturbations, while zonal density and electrostatic potential can still behave independently, as already discussed for the GHM system. Note that, historically, the HW system was derived without proper attention to the zonal response, i.e., with  $C(\Phi - n)$  rather than  $C(\tilde{\Phi} - \tilde{n})$  on the right hand sides of (18) and (19). Consequently, in the original system [13], ZFs were observed only for very large values of  $C$  [28]. Because of this, the current form of the HW system is sometimes referred to as the *modified* Hasegawa-Wakatani model. However, we think that this is the only correct form of the model, and therefore we do not use that terminology in this paper.

We present the HW model here as the minimal model of plasma turbulence because it: i) conserves PV, ii) is driven by an instability whose free energy is the PV gradient, iii) generates zonal flows, iv) saturates by a combination of ZFs and the forward enstrophy cascade, and v) does not seem to result in a condensate state (i.e., the ZF size, which stays constant, is smaller than the largest available scale) even without any large scale dissipation.

In order to solve this system numerically, we need to introduce small scale dissipation terms. Here we use standard diffusion, i.e.  $\nu \nabla^2 \zeta$  and  $D \nabla^2 n$ , with the coefficients set to have the smallest value that results in a saturated state with the given resolution (details are given in [24]).

Another reason we focus on such a simple model is that we can solve for the linear eigenmode problem analytically. In particular, taking the Fourier transforms of the linearised forms of Eqns. (18) and (19) and solving for the resulting linear dispersion relation, we find that the complex eigenfrequency can be written as

$$\omega_k^\pm = \omega_{kr}^\pm + i\gamma_k^\pm = \pm W_k - iA_k, \quad (22)$$

with  $\omega_{kr}^\pm$  the real frequency and  $\gamma_k^\pm$  the growth/damping rate, where  $A_k = C(1 + k^2)/(2k^2)$  and

$$W_k = \frac{A_k}{\sqrt{2}} \left( \frac{k_y}{|k_y|} \sqrt{\sqrt{1 + \left(2\frac{\omega_k^{HM}}{A_k}\right)^2} - 1} + i \sqrt{\sqrt{1 + \left(2\frac{\omega_k^{HM}}{A_k}\right)^2} + 1} \right), \quad (23)$$

where  $\omega_k^{HM} = \kappa k_y / (1 + k^2)$  is the Hasegawa-Mima frequency, and  $k^2 = k_x^2 + k_y^2$ .

Note that, in the large  $C$  limit, if we also set  $\bar{n} \rightarrow 0$ , we recover Eqn. (14) and the PV expression  $q = \tilde{\Phi} - \nabla^2 \Phi - \kappa x$ , since relaxation to adiabaticity becomes very strong, while the energy injection becomes vanishingly small. We can show that the growth rate in this  $C \rightarrow +\infty$  limit scales as  $\gamma_k = k^2 (\omega_k^{HM})^2 / C(1 + k^2)$ , and peaks at  $k_y = \sqrt{2}$ , rather close to the eventual peak of the  $k$ -spectrum, which is dominated by ZFs. This is in contrast to small-scale injection in the GFD case.

## 2. Geophysical case: the Two-Layer QG model

There are a number of similarly ‘simplest’ models in GFD that may be used to describe the baroclinic instability. In these models it is the vertical flow shear that gives rise to the basic linear instability, which can be modelled by considering two layers moving at different speeds. The model that we study here consists of PV conservation equations in each layer [14, 15]:

$$(\partial_t + U_1 \partial_x + \hat{n} \times \nabla \psi_1 \cdot \nabla) q_1 + (\beta + F_1 \Delta U) \partial_x \psi_1 = 0, \quad (24)$$

$$(\partial_t + U_2 \partial_x + \hat{n} \times \nabla \psi_2 \cdot \nabla) q_2 + (\beta - F_2 \Delta U) \partial_x \psi_2 = 0, \quad (25)$$

where  $U_i$  is the east-west velocity of the  $i$ -th layer, such that  $\Delta U = U_1 - U_2$  makes the two layers vertically sheared. In this system, the total PV of the  $i$ -th layer,  $q_i$ , is

$$q_1 = q'_1 + (\beta + F_1 \Delta U) y \quad \text{and} \quad q_2 = q'_2 + (\beta - F_2 \Delta U) y, \quad (26)$$

where the perturbed PV (zonal and non-zonal combined)  $q'_i$  is

$$q'_1 = \nabla^2 \psi_1 + F_1 (\psi_2 - \psi_1) \quad \text{and} \quad q'_2 = \nabla^2 \psi_2 + F_2 (\psi_1 - \psi_2),$$

with  $i = 1, 2$  corresponding to the top and bottom layers respectively. Here,  $\beta + F_1 \Delta U$  and  $\beta - F_2 \Delta U$  represent the background PV gradients, due to planetary vorticity and the vertically sheared background (east-west) mean flows. Using the normalisation  $x/R \rightarrow x$ ,  $y/R \rightarrow y$ ,  $Ut/R \rightarrow t$ ,  $R^2 \beta / U \rightarrow \beta$ ,  $F_i / R^2 \rightarrow F_i$  and finally  $\psi_i R^{-1} U^{-1} \rightarrow \psi_i$ , so that  $q_i R / U \rightarrow q_i$ , and physical parameters from [15], the linear growth rate peaks around the dimensionless

wave-number  $k \approx 0.6$ . Since, for these parameters,  $\beta$  is rather small compared to  $U/R^2$ , the Rossby wave-number  $k_R = \sqrt{\beta/U}$  computed with the imposed jet speed  $U$  is smaller than the wavenumber of the most unstable mode. Thus the box size should be sufficiently large in order to capture the inverse energy cascade, which produces ZFs at large enough scales, where the Rossby wave dynamics can take over. Bottom friction can be included in the equation for  $q_2$  (i.e., a term of the form  $\nu_f \nabla^2 \psi_2$  on the left hand side of Eqn. (25)), as well as viscous dissipation in both equations (i.e.,  $\nu \nabla^2 q_{1,2}$  on the right hand sides of Eqns. (24) and (25)) to remove small-scale potential enstrophy.

Having described the different minimal models that feature the formation of ZFs in both GFD and magnetised plasma physics, in the following section we describe the results of numerical simulations performed to investigate the layering process in each model, which depends on the energy injection scale and zonal response.

### III. FORCED $\beta$ -PLANE TURBULENCE

The definition of PV (i.e.,  $q$ ) in terms of various fields of the system, and its inversion, defines the instability mechanism, while PV conservation provides the physics of flow self-organisation. Using a linear relation between the other fields and the potential (e.g.,  $n_k = (1 + i\delta_k) \Phi_k$  for the Hasegawa-Wakatani system), one obtains a linear inversion rule, which, when substituted into the linearised PV conservation equation, gives the dispersion relation. Using linear inversion, together with the solution of the linear dispersion relation, the PV conservation equation can be written with a (small) linear growth term,  $\gamma_k$  say, representing the effect of the underlying linear instability pumping PV. If  $\gamma_k$  is non-zero only at very small scales and we are interested in the large-scale evolution, we could model the instability as small-scale stochastic forcing and use Eqn. (8) invoking an inverse cascade argument.

In this section, we study the formation of ZFs in the general  $\beta$ -plane framework. First, we consider the classic CHM system, forced at small scales, and then the minimal GFD system with instability, i.e., the QG two-layer model. We then turn to magnetised plasmas with modified zonal response: the GHM system forced at small scales, and the Hasegawa-Wakatani system.

#### A. Standard Charney-Hasegawa-Mima model forced at small scales

Considering the stochastically forced CHM system (6), we perform a  $2048^2$  padded resolution DNS with a box size  $L_x \times L_y = 8\pi \times 8\pi$ ,  $\beta = 1$ , and standard kinematic viscosity with  $\nu = 2 \cdot 10^{-5}$ . The forcing  $f_k$  is taken as a Gaussian ring centred at  $k = 20$ , an amplitude  $A = 10$ , a width  $\sigma_k = 0.5$  and a random phase that changes at a time scale that is five times the shortest wave period (so that the forcing stays coherent on the time scale of the fastest frequency). The simulation is initialised with a Gaussian seed in Fourier space, also with random phases, and the system is evolved up to  $t = 10^4$ . The results are shown in figure 2.

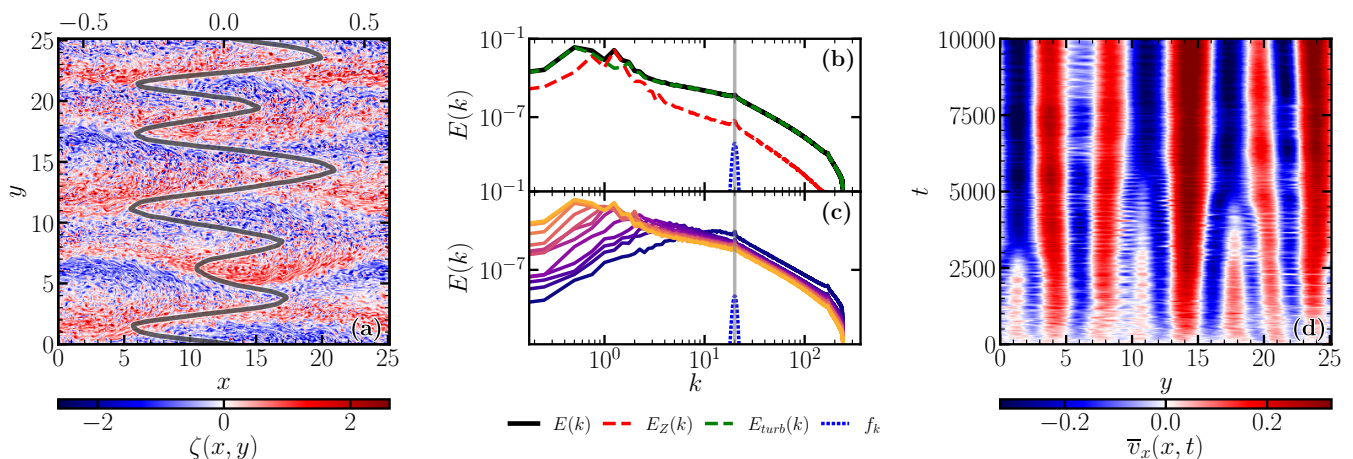


Figure 2. Standard CHM simulation with small-scale forcing. (a) Vorticity snapshot  $\zeta(x, y)$  at the final time step and the zonal velocity profile  $\bar{v}_x$  (grey line). (b) Kinetic energy spectrum  $E(k)$  (black), time averaged over  $7500 < t < 10000$ , decomposed into zonal  $E_Z(k)$  (red) and non-zonal  $E_{turb}(k)$  (green) parts. The forcing around  $k = 20$  (vertical grey line) is in dotted blue. (c) Kinetic energy spectrum at different timesteps, from early stage (blue) to ZFs (yellow). (d) Hovmöller diagram of the zonal velocity profile  $\bar{v}_x$ .

Figure 2a shows a vorticity snapshot  $\zeta(x, y)$  at the final timestep. We can distinguish the self-organised large-scale horizontal zonal flow pattern, coexisting with smaller-scale 2D vortices. The jets are not exactly straight, but are elongated in  $y$ ; this feature may be related to exact solutions of the 2D Euler equation based on Jacobi elliptic functions [29, 30]. The form of the jets is further illustrated in figure 2b, which shows the isotropic spectrum of the kinetic energy  $\mathcal{K} = \sum_k k^2 |\psi_k|^2$  decomposed into zonal ( $k_x = 0$ , red) and non-zonal ( $k_x \neq 0$ , green) parts. The peak of the spectrum at  $k \approx 1$  is dominated by zonal modes  $k_x = 0$ , but larger scales are also populated by non-zonal modes, corresponding to large-scale modulations of zonal jets. In figure 2c, the kinetic energy spectrum is shown at different times (from blue to yellow), where we note the development of the inverse cascade and the formation of the zonal peak. In time, the spectrum reaches even larger scales, meaning that after waiting a sufficient amount of time, a condensate will probably form [31], due to the Rhines scale growing with time [32] in the absence of large-scale friction. In figure 2d, which shows the time evolution of the zonal velocity profile  $\bar{v}_x$ , the progressive merging of the jets can be observed. Oscillations are also visible, related to the modulations of the boundaries of the ZFs.

In short, the zonal pattern that forms in the CHM system is not unidirectional. Instead,  $k_x = 0$  (zonal) modes appear along with other low  $k_x$  modes, giving rise to the elliptical/meandering structure of the jets. Moreover, the width of the jets, which is linked to the Rhines scale [8, 33], increases with time as they merge, until they reach either the box size or they equilibrate with large-scale dissipation [32]. Note that the pattern formation requires a forcing that is both weak and sufficiently slowly varying compared to the linear frequency, in order to allow for resonant interactions to develop.

## B. Instability-driven two-layer QG model

To investigate layering as the nonlinear evolution of an initial linear instability, we perform a  $2048^2$  padded resolution DNS of the two-layer QG model (Eqns. (24) and (25)). Using the same normalisation as [15], the box size is  $L_x \times L_y = 128\pi \times 128\pi$ , with  $\beta = 0.084$ ,  $F_1 = 0.8$ ,  $F_2 = 0.2$ ,  $U_1 = 1$  and  $U_2 = 0$  such that  $\Delta U = 1$ , with standard minimal diffusion at small scales, with viscosity  $\nu = 0.05$ . To retain a minimal model, no bottom friction is included. The system is evolved up to  $t = 10^3$ .

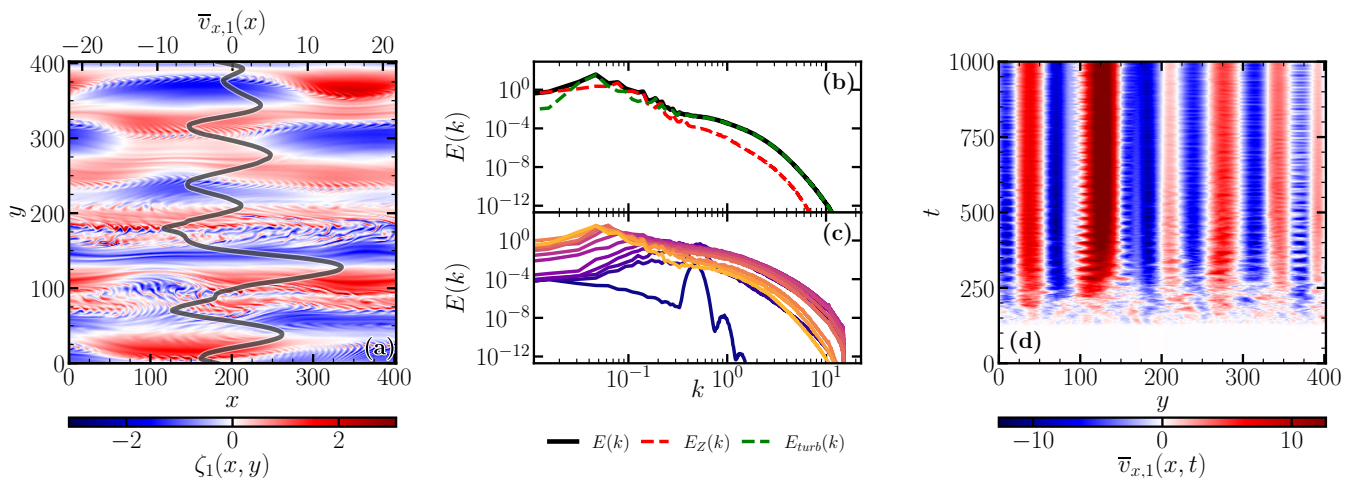


Figure 3. Two-Layer QG model results for the top layer. (a) Vorticity snapshot at the final time step and zonal velocity profile (grey line). (b) Kinetic energy spectrum  $E(k)$  (black) time averaged over  $750 < t < 1000$ , decomposed into zonal  $E_Z(k)$  (red) and non-zonal  $E_{turb}(k)$  (green) parts. (c) Kinetic energy spectrum at different timesteps, from early stage (blue) to ZFs (yellow). (d) Hovmöller diagram of the zonal velocity profile.

Results for the top layer (i.e.,  $i = 1$ ) are presented in figure 3. The vorticity snapshot in figure 3a shows the system at the last time step, where we again observe the large-scale elongated elliptical jet structures, with waves visible at their boundaries. The kinetic energy spectrum in figure 3b shows that the dominant structures are not purely zonal, with multiple peaks of the zonal spectrum corresponding to different zonal widths. The time evolution of the kinetic energy spectrum in figure 3c shows the peak of the linear instability (blue), around  $k = 0.6$ , which then saturates, resulting in an anisotropic inverse energy transfer (violet to yellow). From the spatiotemporal evolution of the zonal velocity profile in figure 3d, we observe that the flows are quite steady and do not undergo any merging after the early times, with oscillations corresponding to wavelike movement of the elliptical boundaries of the jets. Notice that the

evolution here is much quicker than that for the CHM system, probably since the instability makes the system react much faster and stronger than the forcing.

### C. Generalised Hasegawa-Mima model

We now consider the plasma problem, using the GHM equation, with its modified zonal response, forced stochastically at small scales. Note that, as we switch to the plasma convention, the zonal modes correspond to  $k_y = 0$ , or purely  $k_x$  wavenumbers. We perform a DNS of the GHM system (Eqn. 14), with a padded resolution  $2048^2$ , and a box size of  $L_x \times L_y = 20\pi \times 20\pi$ , with  $\beta = 1$ , and  $\nu = 10^{-3}$ , with a forcing centred on  $k = 10$ , of width  $\sigma_k = 1$  and magnitude  $A = 10^{-3}$ . The system is evolved up to  $t = 530$ . The results are shown in figure 4.

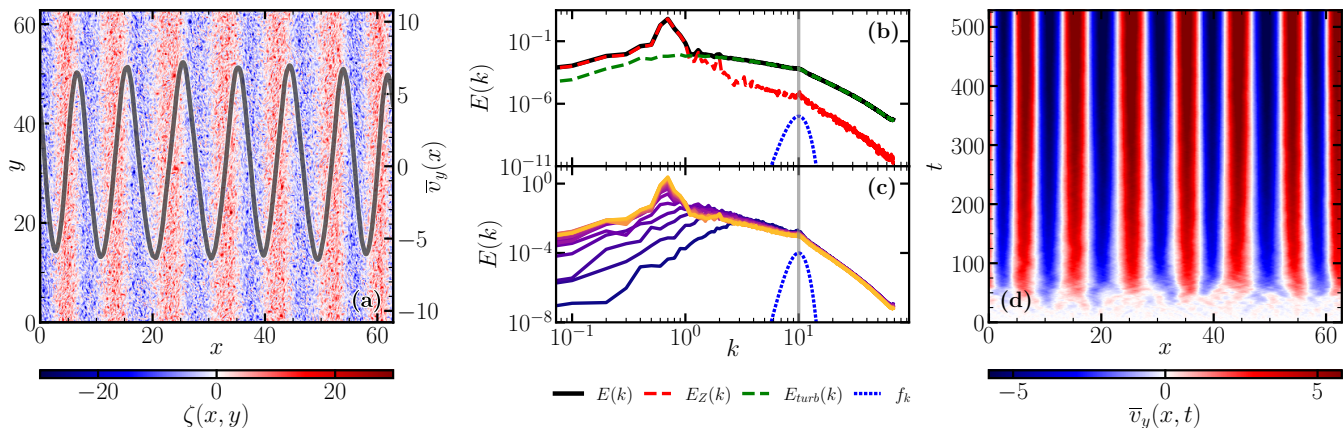


Figure 4. GHM simulation with small-scale forcing. (a) Vorticity snapshot and zonal velocity profile (grey line) at the final time step. (b) Kinetic energy spectrum  $E(k)$  (black) time averaged over  $400 < t < 530$ , decomposed into zonal  $E_Z(k)$  (red) and non-zonal  $E_{turb}(k)$  (green) parts. The forcing, which is around  $k = 10$  (vertical grey line), is in dotted blue. (c) Kinetic energy spectrum at different timesteps, from early stage (blue) to steady ZFs (yellow). (d) Hovmöller diagram of the zonal velocity profile.

The vorticity snapshot and the zonal velocity profile  $\bar{v}_y$  at the last timestep (figure 4a) shows an almost regular pattern, with the jets being completely straight, as a result of the modified zonal response. This is further illustrated in figure 4b, where the kinetic energy spectrum shows that the energy is dominated at large scales by the zonal modes, which corresponds to the peak at  $k_x \approx 0.8$ , with small scales  $k > 2$  dominated by 2D turbulence. In figure 4c, the kinetic energy spectrum is shown at different timesteps (from blue to yellow), where we see a build-up of the inverse cascade, resulting in the emergence of ZFs, corresponding to the dominant peak. Here the ZFs are steady and do not change size during the computation time, as shown in figure 4d.

A key quantity for the formation of ZFs is the so-called Reynolds power, defined as  $P_{Re} \equiv -\int \bar{v}_y \partial_x R dx$ , with  $R \equiv \langle \tilde{v}_x \tilde{v}_y \rangle_y = -\langle \partial_x \tilde{\Phi} \partial_y \tilde{\Phi} \rangle_y$  being the Reynolds stress, which represents the power that goes from 2D turbulence to ZFs (i.e.,  $d\mathcal{K}_Z/dt = P_{Re}$ , where  $\mathcal{K}_Z = (1/2) \int \bar{v}_y^2 dx$  is the zonal kinetic energy). We observed (not shown here) that for forced GHM, the Reynolds power stays positive, meaning that ZFs continue to receive energy. In contrast, the ZFs can actually turn off the drive in the instability-driven case.

We also tried forcing the GHM system at large scales, using the linear growth rate from the Hasegawa-Wakatani system, which introduces an *ad hoc* linear instability into the system. Zonal flows are generated as usual, but they do not lead to a saturated state in which they dominate, contrary to when the system is forced at small scales. Instead, the flows coexist with strong eddies, especially dipoles, which progressively dominate the system. Again, this is because the ZFs cannot turn off the energy drive provided by an *ad hoc* linear instability.

## IV. THE HASEGAWA-WAKATANI SYSTEM

In this section, we discuss the formation of zonal flows in the Hasegawa-Wakatani system, governed by Eqns. (18) and (19), driven by linear instability, where the ratio of the adiabaticity parameter to the mean density gradient  $C/\kappa$  plays the role of the control parameter. First, we look at the standard case  $C/\kappa = 1$ , which exhibits stationary ZFs dominating the system. We then study the transition from 2D turbulence to quasi-1D ZFs as  $C/\kappa$  is varied. Finally,

we discuss the saturation mechanism in the system when it is dominated by ZFs, and how this relates to the layer formation.

### A. The standard ( $C/\kappa = 1$ ) case.

We perform a DNS of the Hasegawa-Wakatani system with a padded resolution  $4096^2$  and parameters  $C = 1$  and  $\kappa = 1$ , on a box size  $L_x \times L_y = 40\pi/k_{y0} \times 40\pi/k_{y0}$ , where  $k_{y0} \approx 1.3$  is the poloidal wavenumber of the most unstable mode from the linear dispersion relation (22), which acts as a proxy for the energy injection scale. We introduce small-scale dissipation using standard diffusion terms  $\nu \nabla^2 \tilde{\zeta}$  and  $D \nabla^2 \tilde{n}$  respectively for vorticity and density, with  $\nu = D = 3.1 \cdot 10^{-4}$ , in order to compensate energy injection by the linear instability. Note that no dissipation is applied to the zonal fields, either at small or large scales, since we observe that the system is able to converge regardless. The system is evolved up to  $t = 950$ .

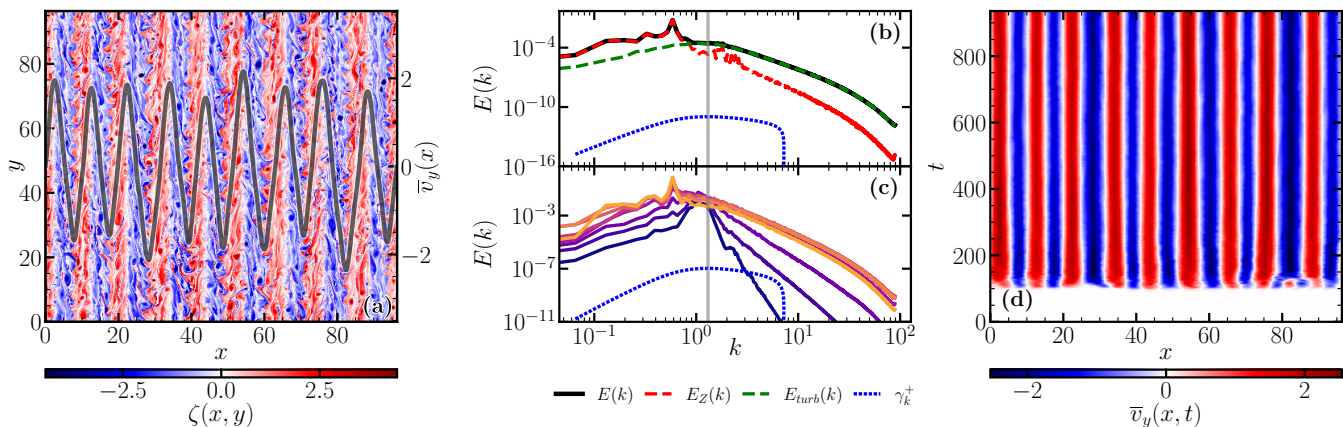


Figure 5. HW simulation with  $C = 1$ ,  $\kappa = 1$ . (a) Vorticity snapshot and zonal velocity profile (grey line) at the final time step. (b) Kinetic energy spectrum (black), time averaged over  $475 < t < 950$ , decomposed into zonal (red) and non-zonal (green) parts. The positive part of the growth rate, which is maximised at  $k_{y0} \approx 1.3$  (vertical grey line) is in dotted blue; the growth rate becomes negative at small scales owing to viscous dissipation. (c) Kinetic energy spectrum at different timesteps, from the saturation of the linear instability (blue) to the steady ZFs (yellow). (d) Hovmöller diagram of the zonal velocity profile.

The simulation results are presented in figure 5. The vorticity snapshot in figure 5a shows a system dominated by quasi-periodic ZFs, similar to the GHM system forced at small scales, with 2D eddies of sizes similar to the radial width of the jets. The kinetic energy spectrum (figure 5b) illustrates this final state, where large scales ( $k < 0.8$ ) are dominated by ZFs (dashed red), with the peak at  $k \approx 0.6$  corresponding to the mean radial width of ZFs, while smaller scales are dominated by 2D turbulence, with a peak close to that of the most unstable mode  $k_{y0}$ , which is only two times smaller than the zonal spectrum peak. The time evolution of the kinetic energy spectrum (figure 5c) shows that the energy, initially concentrated around the most unstable mode when the linear instability saturates, progressively moves to the peak of the zonal spectrum.

Finally, the evolution of the zonal profile (figure 5d) shows that the ZFs are extremely steady, with typical width and spacing of jets that are not dependent on the box size. Comparing the previous results for CHM to GHM, along with the results on the two-layer QG model and earlier results on the Hasegawa-Wakatani model with standard zonal response [28], we argue that the steadiness of the jets is a consequence of the modified zonal response above anything else. Furthermore, in this case, the Reynolds power (not shown here) is zero in the steady state. Once established, ZFs locally modify the linear properties of the system. Energy injection by the instability is weakened and shifted to smaller scales, where it is removed by enstrophy dissipation.

### B. The 2D to quasi-1D transition, and the transition scale

As discussed above, the formation of ZFs in the Hasegawa-Wakatani system depends on whether or not the control parameter  $C/\kappa$  is larger than the critical value  $(C/\kappa)_c \approx 0.1$  [22–24]. If  $C/\kappa < 0.1$ , the system evolves to one of 2D eddies, with typical sizes slightly larger than that of the most unstable mode (e.g., see figure 3 from [24] for an illustration), in a state that can be characterised as disordered, or ‘hot’, from a thermodynamical perspective. In

contrast, for  $C/\kappa > 0.1$ , one finds the system dominated by ZFs, as discussed above for  $C/\kappa = 1$ , which becomes quasi-1D. This regime is more organised and can be seen as a ‘cold’ crystalline-like structure.

This ‘phase transition’ between the two regimes can be studied systematically by quantifying the fraction of zonal to total kinetic energy  $\Xi_\kappa = \mathcal{K}_Z/\mathcal{K}$ , corresponding to the parameter ( $0 \leq \Xi_\kappa \leq 1$ ), when scanning the parameter  $C/\kappa$ . Shown in figure 6a, such a scan exhibits a sharp transition at approximately  $C/\kappa \approx 0.1$ , which clearly separates the 2D turbulent state (low zonal flow level, marked in blue) from the zonal-flow-dominated state (zonal flow level close to 100%, marked in orange).

Furthermore, slowly increasing and then decreasing the order parameter around the transition point  $C/\kappa \approx 0.1$ , while waiting for a time much larger than the instability growth rate, thus performing an adiabatic transformation, one is able to observe a hysteresis loop in the transition from the zonal state back to the turbulent state [24], as shown in figure 6b. From the perspective of phase transition, this means that once zonal flows have been formed, additional latent heat is required in order to destroy them, somewhat similar, for example, to crystal melting.

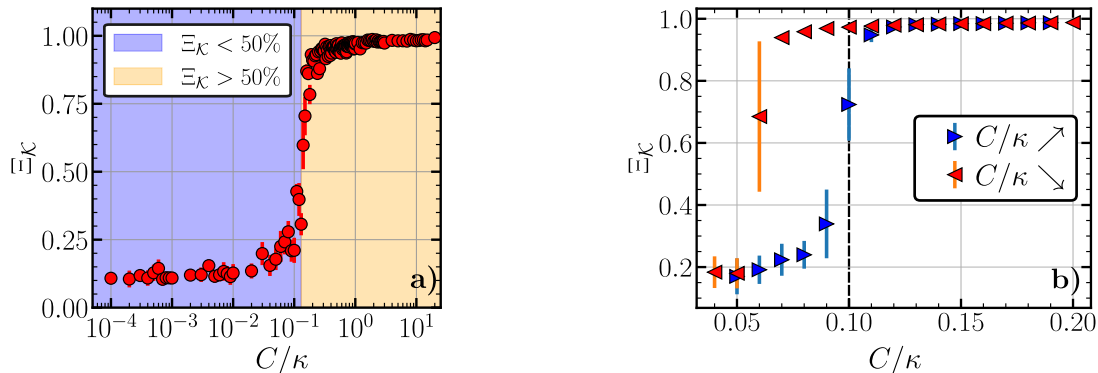


Figure 6. Transition of the zonal flow level in the HW system on varying  $C/\kappa$  (with  $\kappa = 1$ ). (a) Individual scans of  $C/\kappa$ . (b) Hysteresis loop obtained by slowly increasing (blue) and then decreasing (red)  $C$  in one simulation. The dotted line denotes the transition point  $C/\kappa \approx 0.1$

While there is still not a complete understanding of the actual mechanism for the transition and the underlying hysteresis, it can be interpreted in ways similar to the 3D to quasi-2D transitions [34] observed in thin layer turbulence [35] or in rotating turbulent flows [36, 37], using here the existence of a third invariant in  $\beta$ -plane turbulence, namely *zonostrophy* [19, 20, 38, 39].

The transition between 2D turbulence and ZFs can also be discussed using a spectral perspective on defining the *zonostrophy parameter* [40, 41] as the ratio  $R_\beta = k_\beta/k_{peak}$  between the energy containing scale  $1/k_{peak}$  (i.e., the Rhines scale in  $\beta$ -plane turbulence) and the transition scale  $1/k_\beta$  at which the Rossby/drift wave frequency is equal to the inverse eddy turnover time. When  $R_\beta > 1$ , the energy spectrum peak lies well in the wave turbulence regime and the system is dominated by ZFs. On the contrary, for  $R_\beta < 1$  energy is contained in the 2D turbulence scales.

However, in the case of HW, the definition of zonostrophy (or zonostrophy parameter) is not trivial, since the dispersion relation yields complex eigenvalues and thus a growth rate (which generally makes it difficult to apply the weak wave turbulence framework). Furthermore, this argument does not explain either the sharp transition, or the exact transition point, the fact that ZFs have a defined size and amplitude (instead of being a condensate), or the presence of the hysteresis loop. All these pending questions seem tied up altogether.

### C. Relaxation and spreading: flux-driven HW system

In all the examples investigated above, the layering process was observed in the *fixed gradient* framework, where the background PV gradient, which acts as the free energy source, is fixed in time and imposed on the system. This corresponds to assuming scale separation between the turbulence and the mean gradient. In particular, the mean density gradient does not evolve through a transport equation, even though turbulence generates a net particle flux in the outward radial direction. For the HW system, a more physically appropriate description can be achieved in the particle *flux-driven* framework, where the mean gradient is now evolved by a transport equation, involving the turbulent particle flux along with particle sources [42, 43]:

$$\partial_t n_r + \partial_x \Gamma_n = S_n(x, t), \quad (27)$$

where  $n_r = -\kappa(t)x + \bar{n}$  is the total radial profile (i.e., the sum of mean and zonal profiles),  $\Gamma_n = -\langle \tilde{n} \partial_y \tilde{\Phi} \rangle_y$  is the turbulent particle flux along the radial direction, and  $S_n$  is the particle source. Note that we could also introduce neoclassical diffusion through a term  $D_{neo} \partial_x^2 n_r$  acting on the radial profile. More generally, Eqn. (19) can be formulated to include a mean  $\mathbf{E} \times \mathbf{B}$  velocity profile and its relaxation towards a neoclassical flow [44].

In the fixed gradient system, the transition between 2D turbulence and ZFs is studied by performing scans in  $C/\kappa$ , with the control parameter thus kept fixed in a given simulation (except for the hysteresis loop). In the flux-driven case, in contrast, since the mean gradient  $\kappa(t)$  evolves because of particle transport, described by Eqn (27), and the control parameter  $C/\kappa(t)$  changes in time, the zonal flow level is a result of the balance between the turbulent flux and the external particle source, which sets the mean gradient. Since ZFs can, in turn, affect the turbulent flux through shear suppression, this results in a complex feedback loop that is absent in fixed gradient simulations. However, the zonal vorticity profile is still ‘free’ in the fixed gradient formulation, so it can compensate for some of the missing elements.

In the flux-driven case, given an adiabaticity parameter  $C$ , it is the mean gradient  $\kappa_c = C/0.1$  that defines a local threshold between a marginal stable state dominated by ZFs ( $\kappa < \kappa_c$ ), where the turbulent flux is strongly suppressed and relaxation slows down considerably, and the 2D turbulent state.

Close to the marginal threshold, with a low particle source, the feedback loop between profile relaxation towards the stable state and feeding of the particle source, which increases the mean gradient, is reminiscent of self-organised criticality in sandpile models [45–47]. As a result, time series of the density profile close to marginality exhibit a  $1/f$  power law scaling (not shown here). Around the threshold  $\kappa_c$ , different imposed particle fluxes result in very similar mean gradients  $\kappa$ . This is due to different zonal flow levels obtained for similar values of the control parameter  $C/\kappa$ , which is a manifestation of the hysteresis loop in the flux-driven system.

## V. CONCLUSION

Having studied various forced and instability-driven formulations of  $\beta$ -plane turbulence in geophysical and plasma settings, with different zonal flow responses, we conclude that, while the preference for layering is universal, the detailed mechanisms of staircase formation, as well as saturation, are different between forced and instability-driven systems, with the nature of the zonal response playing a key role. Nonetheless, there is a common theme in all the models that we have considered; they all result in PV staircases consisting mainly of zonal flows.

The general mechanism of layering, when PV is slowly injected, is that the gradients increase until the system transitions into a high flux turbulent state, either through a linear instability or a nonlinear phase transition. Then, it relaxes back to the critical state, as a result of this enhanced flux activity, which is linked to self-organised criticality/bistability through avalanches. While we think of self-organisation and layering usually in terms of profiles of density or temperature, in the plasma context, when formulated in terms of PV, vorticity self-organisation is also key. This allows even a fixed gradient model to ‘relax’ its PV, through its vorticity evolution, as the only freely evolving channel for the PV in such a model. In this sense, the differences between instability-driven and stochastically-forced systems are more qualitative in that the instability-driven system can turn off the energy injection, as a result of layering, while the stochastic system needs explicit sinks in order to saturate properly.

There is also the important effect of the zonal flow response. With the standard response, the resulting flows appear as very elongated structures with elliptical jets. In contrast, for the modified zonal flow response, the resulting flows are really 1D and tend to be very stationary. This difference can be observed both between the standard and modified CHM systems, or between the Hasegawa-Wakatani and the two-layer QG models.

On considering the saturated state of the Hasegawa-Wakatani system, with minimal dissipation, we find that the system exhibits a phase transition around  $C/\kappa \approx 0.1$ , with a hysteresis loop that suggests that, once formed, the zonal flows require more energy injection to collapse. We further observe that the generic saturation mechanism, without large-scale friction, for example for a moderate value of  $C/\kappa = 1.0$ , requires both the suppression of the instability by ZFs and a 2D forward enstrophy cascade with small-scale dissipation, with a steady state that has zero net Reynolds power. This happens in a very coordinated way, in which different parts of the zonal profile either contribute to flattening of the PV gradient or to generating sufficient shear suppression that the generated fluctuations are rapidly scattered to small scales, all happening without generating any momentum flux.

Finally, note that a system driven by a constant gradient of some quantity (usually the PV itself, but sometimes another background can play a role), is fundamentally different from a *flux-driven* system. Driven by sources and sinks, such a system can saturate by relaxing the background gradients that drive small-scale motions, providing a further mechanism for staircase formation, in addition to those for forced or instability-driven systems.

## ACKNOWLEDGMENT

The authors thank the Isaac Newton Institute for Mathematical Sciences, Cambridge, for support and hospitality during the programme 'Anti-diffusive dynamics: from sub-cellular to astrophysical scales', which was supported by EPSRC grant EP/R014604/1. This work was granted access to the Jean Zay super-computer of IDRIS under the allocation AD010514291R2 by GENCI, and has been carried out within the framework of the EUROfusion Consortium, funded by the European Union *via* the Euratom Research and Training Programme (Grant Agreement No 101052200 — EUROfusion) and within the framework of the French Research Federation for Fusion Studies. Y.S. and G.D.P. acknowledge that this work was partially supported by a grant from the Simons Foundation. The authors acknowledge stimulating discussions with participants at the 2025 Festival de Théorie in Aix-en-Provence.

- 
- [1] W. Horton and A. Hasegawa. Quasi-two-dimensional dynamics of plasmas and fluids. *Chaos*, 4:227–251, Jun 1994. doi:10.1063/1.166049.
  - [2] P. H. Diamond, S.-I. Itoh, K. Itoh, and T. S. Hahm. Zonal flows in plasma – a review. *Plasma Phys. Controlled F.*, 47(5):R35–R161, 2005. doi:10.1088/0741-3335/47/5/R01.
  - [3] Ö. D. Gürçan and P. H. Diamond. Zonal flows and pattern formation. *J. Phys. A*, 48(29):293001, 2015. doi:10.1088/1751-8113/48/29/293001.
  - [4] P. B. Rhines and W. R. Young. Homogenization of potential vorticity in planetary gyres. *J. Fluid Mech.*, 122(September):347 – 367, 1982.
  - [5] G. Dif-Pradalier, G. Hornung, Ph. Ghendrih, Y. Sarazin, F. Clairet, L. Vermare, P. H. Diamond, J. Abiteboul, T. Cartier-Michaud, C. Ehrlacher, D. Estève, X. Garbet, V. Grandgirard, Ö. D. Gürçan, P. Hennequin, Y. Kosuga, G. Latu, P. Maget, P. Morel, C. Norscini, R. Sabot, and A. Storelli. Finding the elusive  $\mathbf{E} \times \mathbf{B}$  staircase in magnetized plasmas. *Phys. Rev. Lett.*, 114:085004, Feb 2015. doi:10.1103/PhysRevLett.114.085004.
  - [6] J. G. Charney. On the scale of atmospheric motions. *Geophys. Publ. Oslo*, 17:1–17, 1948.
  - [7] A. Hasegawa and K. Mima. Pseudo-three-dimensional turbulence in magnetized nonuniform plasma. *Phys. Fluids*, 21(1):87–92, January 1978. doi:10.1063/1.862083.
  - [8] Peter B. Rhines. Waves and turbulence on a beta-plane. *J. Fluid Mech.*, 69(03):417–443, 1975.
  - [9] ME McIntyre and WA Norton. Potential vorticity inversion on a hemisphere. *J. Atmos. Sci.*, 57(9):1214–1235, 2000.
  - [10] M. E. McIntyre. Potential-vorticity inversion and the wave-turbulence jigsaw: some recent clarifications. *Adv. Geosci.*, 15:47–56, 2008. URL: <https://adgeo.copernicus.org/articles/15/47/2008/>, doi:10.5194/adgeo-15-47-2008.
  - [11] W. Horton, B. G. Hong, and W. M. Tang. Toroidal electron temperature gradient driven drift modes. *Phys. Fluids*, 31(10):2971–2983, October 1988. doi:10.1063/1.866954.
  - [12] A. I. Smolyakov and P. H. Diamond. Generalized action invariants for drift waves-zonal flow systems. *Phys. Plasmas*, 6(12):4410–4413, 1999. doi:10.1063/1.873725.
  - [13] A. Hasegawa and M. Wakatani. Plasma edge turbulence. *Phys. Rev. Lett.*, 50(9):682–686, February 1983. doi:10.1103/PhysRevLett.50.682.
  - [14] G. R. Flierl. Models of vertical structure and the calibration of two-layer models. *Dynam. Atmos. Oceans*, 2(4):341–381, August 1978. doi:10.1016/0377-0265(78)90002-7.
  - [15] L. Wang, M. Jansen, and R. Abernathy. Eddy phase speeds in a two-layer model of quasigeostrophic baroclinic turbulence with applications to ocean observations. *J. Phys. Oceanogr.*, 46(6):1963–1985, June 2016. doi:10.1175/JPO-D-15-0192.1.
  - [16] B. B. Kadomtsev. *Plasma Turbulence*. Academic Press, London, UK, 1965.
  - [17] J. Pedlosky. *Geophysical Fluid Dynamics*. Springer-Verlag, New York, 2nd edition, 1987.
  - [18] A. M. Balk, S. V. Nazarenko, and V. E. Zakharov. Nonlocal turbulence of drift waves. *Phys. Lett. A*, 146(4):217, 1990.
  - [19] S. Nazarenko and B. Quinn. Triple cascade behavior in quasigeostrophic and drift turbulence and generation of zonal jets. *Phys. Rev. Lett.*, 103(11):118501, September 2009. doi:10.1103/PhysRevLett.103.118501.
  - [20] C. Connaughton, S. Nazarenko, and B. Quinn. Rossby and drift wave turbulence and zonal flows: The Charney-Hasegawa-Mima model and its extensions. *Phys. Rep.*, 604:1–71, 2015. doi:10.1016/j.physrep.2015.10.009.
  - [21] B. Dubrulle and S. Nazarenko. Interaction of turbulence and large-scale vortices in incompressible 2d fluids. *Physica D*, 110(1-2):123–138, 1997.
  - [22] R. Numata, R. Ball, and R. L. Dewar. Bifurcation in electrostatic resistive drift wave turbulence. *Phys. Plasmas*, 14(10):102312, October 2007. doi:10.1063/1.2796106.
  - [23] F. Grander, F. F. Locker, and A. Kendl. Hysteresis in the gyrofluid resistive drift wave turbulence to zonal flow transition. *Phys. Plasmas*, 31(5):052301, May 2024. doi:10.1063/5.0202720.
  - [24] P. L. Guillon and Ö. D. Gürçan. Phase transition from turbulence to zonal flows in the Hasegawa–Wakatani system. *Phys. Plasmas*, 32(1):012306, January 2025. doi:10.1063/5.0242282.
  - [25] A. M. Dimits, B. I. Cohen, N. Mattor, W. M. Nevins, D. E. Shumaker, S. E. Parker, and C. Kim. Simulation of ion temperature gradient turbulence in tokamaks. *Nucl. Fusion*, 40(3Y):661, March 2000. doi:10.1088/0029-5515/40/3Y/329.
  - [26] G K Vallis. *Atmospheric and Oceanic Fluid Dynamics: Fundamentals and Large-scale Circulation*. Cambridge University Press, Cambridge, UK, first edition, 2006.

- [27] A. I. Smolyakov, P. H. Diamond, and V. I. Shevchenko. Zonal flow generation by parametric instability in magnetized plasmas and geostrophic fluids. *Phys. Plasmas*, 7(5):1349–1351, 2000.
- [28] Andrey V. Pushkarev, Wouter J. T. Bos, and Sergey V. Nazarenko. Zonal flow generation and its feedback on turbulence production in drift wave turbulence. *Phys. Plasmas*, 20(4):042304, 2013. doi:10.1063/1.4802187.
- [29] Michael C. Haslam, Christopher J. Smith, Ghada Alobaidi, and Roland Mallier. Some nonlinear vortex solutions. *Int. J. Differ. Equ.*, 2012(none):1 – 10, 2012. doi:10.1155/2012/929626.
- [30] Ö. D. Gürcan. Structure dominated two-dimensional turbulence: formation, dynamics and interactions of dipole vortices. *J. Phys. A*, 56(28):285701, jun 2023. URL: <https://dx.doi.org/10.1088/1751-8121/acdc6b>, doi:10.1088/1751-8121/acdc6b.
- [31] R.K. Scott. The limits of  $\beta$ -plane turbulence. *J. Fluid Mech.*, 973:A33, 2023. doi:10.1017/jfm.2023.672.
- [32] S. Sukoriansky, N. Dikovskaya, and B. Galperin. On the arrest of inverse energy cascade and the Rhines scale. *J. Atmos. Sci.*, 64(9):3312–3327, September 2007. doi:10.1175/JAS4013.1.
- [33] G. K. Vallis and M. E. Maltrud. Generation of mean flows and jets on a beta plane and over topography. *J. Phys. Oceanogr.*, 23(7):1346–1362, July 1993. doi:10.1175/1520-0485(1993)023<1346:GOMFAJ>2.0.CO;2.
- [34] A. Alexakis and L. Biferale. Cascades and transitions in turbulent flows. *Phys. Rep.*, 767–769:1–101, November 2018. doi:10.1016/j.physrep.2018.08.001.
- [35] S. J. Benavides and A. Alexakis. Critical transitions in thin layer turbulence. *J. Fluid Mech.*, 822:364–385, July 2017. doi:10.1017/jfm.2017.293.
- [36] A. Seshasayanan, K. and Alexakis. Condensates in rotating turbulent flows. *J. Fluid Mech.*, 841:434–462, April 2018. doi:10.1017/jfm.2018.106.
- [37] S. Gomé and A. Frishman. Waves drive the rise and fall of 2D flows in rotating turbulence. *preprint*, September 2025. doi:10.48550/arXiv.2509.18323.
- [38] A. M. Balk. A new invariant for Rossby wave systems. *Phys. Lett. A*, 155(1):20–24, April 1991. doi:10.1016/0375-9601(91)90501-X.
- [39] A. M. Balk, S. V. Nazarenko, and V. E. Zakharov. New invariant for drift turbulence. *Phys. Lett. A*, 152(5):276–280, January 1991. doi:10.1016/0375-9601(91)90105-H.
- [40] R. K. Scott and D. G. Dritschel. The structure of zonal jets in geostrophic turbulence. *J. Fluid Mech.*, 711:576–598, November 2012. doi:10.1017/jfm.2012.410.
- [41] Ö. D. Gürcan. Internally driven  $\beta$ -plane plasma turbulence using the Hasegawa-Wakatani system. *preprint*, March 2024. doi:10.48550/arXiv.2403.09911.
- [42] O. Panico, Y. Sarazin, P. Hennequin, Ö. D. Gürcan, R. Bigué, G. Dif-Pradalier, X. Garbet, P. Ghendrih, R. Varennes, and L. Vermare. On the importance of flux-driven turbulence regime to address tokamak plasma edge dynamics. *J. Plasma Phys.*, 91(1):E26, February 2025. doi:10.1017/S0022377824001624.
- [43] P. L. Guillon, Ö. D. Gürcan, G. Dif-Pradalier, Y. Sarazin, and N. Fedorczak. Flux-driven turbulent transport using penalisation in the Hasegawa-Wakatani system. *J. Plasma Phys.*, 91(5):E145, October 2025. doi:10.1017/S0022377825100895.
- [44] L. Chóné, P. Beyer, Y. Sarazin, G. Fuhr, C. Bourdelle, and S. Benkadda. Mechanisms and dynamics of the external transport barrier formation in non-linear plasma edge simulations. *Nucl. Fusion*, 55(7):073010, June 2015. doi:10.1088/0029-5515/55/7/073010.
- [45] P. Bak, C. Tang, and K. Wiesenfeld. Self-organized criticality: an explanation of the  $1/f$  noise. *Phys. Rev. Lett.*, 59(4):381–384, July 1987. doi:10.1103/PhysRevLett.59.381.
- [46] T. Hwa and M. Kardar. Avalanches, hydrodynamics, and discharge events in models of sandpiles. *Phys. Rev. A*, 45(10):7002–7023, May 1992. doi:10.1103/PhysRevA.45.7002.
- [47] B. A. Carreras, D. Newman, V. E. Lynch, and P. H. Diamond. A model realization of self-organized criticality for plasma confinement. *Phys. Plasmas*, 3(8):2903–2911, August 1996. doi:10.1063/1.871650.